P1.5   THE AP GROUND CLUTTER MITIGATION SCHEME FOR THE WSR-88D

Cathy Kessinger, Scott Ellis, Joseph Van Andel, Jaimi Yee,
and John Hubbert
National Center for Atmospheric Research
P.O. Box 3000

Boulder, CO 80305

1. Introduction

Implementation of the AP Clutter Mitigation Scheme is underway within the WSR-88D system as part of the Open Radar Product Generator (ORPG; Saffle et al. 2001). Once fully implemented, this scheme will improve the radar base data quality by identification and removal of ground clutter produced under anomalous propagation (AP) conditions. The current WSR-88D quality control system removes ground clutter that is present during normal propagation conditions by application of clutter bypass maps. AP ground clutter requires manual application of additional clutter filters. The AP Clutter Mitigation Scheme is working toward full automation of ground clutter filter specification and control. The first step in this implementation was achieved when the AP Clutter Detection Algorithm (APDA) was deployed during Build 2 of the ORPG in September 2002. Output from the APDA is available for perusal on the ORPG Clutter Filter Control panel and is expressed in terms of "clutter likelihood values" between 0-100, with 100 meaning that clutter is very likely present.

The WSR-88D AP Clutter Mitigation Scheme (Ellis et al. 2003; Kessinger et al. 2002) consists of three parts: 1) the Radar Echo Classifier (REC) of which the APDA is one module and the Precipitation Detection Algorithm (PDA) is a second module, 2) the Reflectivity Compensation Scheme (Z-Comp), and 3) clutter filter control.

The Enhanced Preprocessing Subsystem (EPRE; O'Bannon and Ding, 2003) is an enhanced version of the Precipitation Pre-processing Subsystem (PPS; Fulton et al. 1998; O'Bannon 1998) and is used to compute radar-derived rainfall estimates. The EPRE was implemented in ORPG

Build 5 in spring 2004 and uses the APDA to remove clutter from the hybrid reflectivity scan. Once fully deployed within the ORPG, output from the APDA, the PDA and the Z-Comp will be input into the EPRE. The PDA and the Z-Comp output will further enhance EPRE precipitation estimates by correcting for the clutter filter bias in the reflectivity within precipitation-only echoes.

The Sigmet Corporation RVP8 digital signal processor will be installed on WSR-88D systems as part of the Open Radar Data Acquisition (ORDA; Elvander et al. 2001). The RVP8 has also been installed on the NCAR S-band dual-Polarization radar (S-Pol) (Keeler et al. 2000) as a parallel processor (Keeler et al. 2003). The RVP8 processor will allow the use of spectral domain processing and will facilitate greater improvement in base data quality. Modification of the AP Clutter Mitigation Scheme to accommodate the new ORDA processor is planned and some preliminary results are presented.

The United Arab Emirates (UAE) has a network of five Enterprise Electronics Corporation (EEC) C-band radars. Atmospheric conditions leading to anomalous propagation of the radar beam are severe in the summer and lead to extensive AP ground clutter and sea clutter contamination in the base data fields. The UAE funded an effort to improve the quality of the radar base data fields through the use of the REC to remove ground and sea clutter. A Sea Clutter Detection Algorithm (SCDA) was developed and has been deployed on their radars as has a modified version of the APDA (called the mAPDA). Results are presented.

Corresponding author address: Cathy Kessinger, NCAR, P.O.
Box 3000, Boulder, CO 80307; email: kessinge@ucar.edu

2. The WSR-88D AP Clutter Mitigation Scheme

2.1. Radar Echo Classifier

The radar echo classifier (REC) is an expert system that uses "fuzzy-logic", data fusion techniques (Kosko, 1992) to estimate the type of scatterer measured by a radar and uses the moment fields of reflectivity, radial velocity and spectrum width as input. The REC as devised for the WSR-88D is described in detail in Kessinger, et al. (2003). The two WSR-88D ORPG algorithms are the AP Detection Algorithm (APDA) that classifies regions of ground clutter and the Precipitation Detection Algorithm (PDA) that classifies regions of convective and stratiform precipitation. The APDA and the PDA were developed using data from several WSR-88Ds and the S-Pol (Kessinger et al. 1999). Real-time deployment of the REC has been accomplished on the S-Pol at various field experiments since June 2000.

2.2. Reflectivity Compensation Scheme

The Reflectivity Compensation scheme (Z-Comp) uses a Gaussian approximation for the precipitation spectra and a simulated WSR-88D clutter filter to estimate the correction to offset the clutter-filter-induced (negative) bias in the reflectivity. Details of the algorithm design and implementation are in Ellis (2001). The Z-Comp method has been tested quantitatively using WSR-88D time-series data (aka Archive 1) collected at the Memphis (KNQA) WSR-88D and has been run operationally on the S-Pol since 2001.

Within the AP Clutter Mitigation Scheme, output from the REC APDA and the PDA determine where the Z-Comp scheme is applied such that only regions of precipitation are compensated. This prevents undesired compensation of reflectivity values within ground clutter return.

3. REC Transition from the ORPG to the ORDA

For the ORDA, the AP Clutter Mitigation Scheme will be adapted to incorporate spectral domain processing techniques. The Sigmet Corporation's RVP8 digital signal processor will be the new processor for the WSR-88D and is planned for deployment on Build 8. The RVP8 has also been installed on the NCAR S-Pol (Keeler et al, 2003). The RVP8 allows various spectral processing techniques to be used for clutter filter removal that should lead to additional enhancements in radar data quality. Having RPV8 on both the S-Pol and the WSR-88D will expedite technique development and deployment.

The ability to create new feature fields for input into the REC is enhanced with spectral domain processing. Two new variables have been designed based on spectral characteristics and were input into the APDA. Membership functions were devised and results compared to the APDA without the spectral variables to show the improvements possible in the spectral domain.

Figure 1 shows an idealized power spectrum, $F(g_i)$, where g_i is the velocity index with g_n corresponding to the Nyquist velocity and where $F(g_i)$ is the power at the g_i velocity index. In this simple example, it is assumed that the duration of the time series samples yields a velocity increment (delta g) of about 0.5 m s^{-1} such that the majority of the clutter power is contained in the spectral points g_0, g_{-1} and g_1. The large broad "hump" to the left of the clutter is precipitation return. Comparison of the power values at various points in the spectra will yield useful information and help to discriminate clutter from precipitation.

For example, calculating the "clutter power" (C_p) can be done as follows:

$$C_p = \sum \; [F(g_0) + F(g_{-1}) + F(g_{+1})]) \qquad \text{Eq. 1}$$

where $F(g_i)$ corresponds to the power at the ith velocity index. The C_p contains the power that is indicated by the blue region in Fig. 1. Calculating the "power near zero" (P_{nz}) is done as follows:

$$P_{nz} = \sum \; [F(g_{-3}) + F(g_{-2}) + F(g_2) + F(g_3)]. \qquad \text{Eq. 2}$$

The P_{nz} contains the power to either side of the C_p region and is indicated by the green regions in Fig. 1. The "total power" ("P_{tot}") is the summation of the power at all velocity indices and is calculated as follows:

$$P_{tot} = \sum_{-n}^{n} F(g_i) \qquad \text{Eq. 3}$$

where i is summed from –n to +n. Using these equations, two new variables are defined, termed "Ratio 1" and "Ratio 2", that are calculated as follows:

$$\text{Ratio 1} = C_p/(P_{tot} - C_p) \qquad \text{Eq. 4}$$

and

$$\text{Ratio 2} = C_p/P_{nz}. \qquad \text{Eq. 5}$$

These variables should enable better discrimination between convective precipitation return and clutter return. Clutter typically has a narrow spectrum while convective precipitation has a broad spectrum. Stratiform precipitation is not being considered in this discussion. When Ratio 1 is large, then the majority of the power is at the velocity index g_0 and may be a good indicator of clutter return. Likewise, when Ratio 2 is large, this indicates that the majority of the power is at the g_0 velocity index rather than in the P_{nz} region and suggests a narrow spectrum at g_0. Clutter return may be indicated when both ratios are large.

Using time series data from the Norman WSR-88D (KOUN) radar, both ratios are calculated. The variables P_{tot}, C_p and P_{nz} are shown in Fig. 2 with the moment data. As suggested, these variables show a good ability to discriminate between precipitation and clutter return in this example. The Ratio 1 and Ratio 2 fields (Fig. 3) show that both Ratios tend to be large within clutter when compared to precipitation return.

After devising appropriate membership functions for Ratios 1 and 2, the spectral variables were input into the APDA as additional feature fields. To distinguish the original APDA without spectral domain variables from the APDA with spectral domain variables, the latter will be referred to as APDA-spectral. As is seen in Fig. 4 especially in the region enclosed by the red ovals, the APDA-spectral has better performance at discriminating between precipitation and clutter echoes than the original APDA. Less precipitation is incorrectly removed using the APDA-spectral.

These results are very encouraging for the migration of the APDA into the ORDA environment with resultant improvements in radar data quality. Development is continuing, additional results will be presented at the conference.
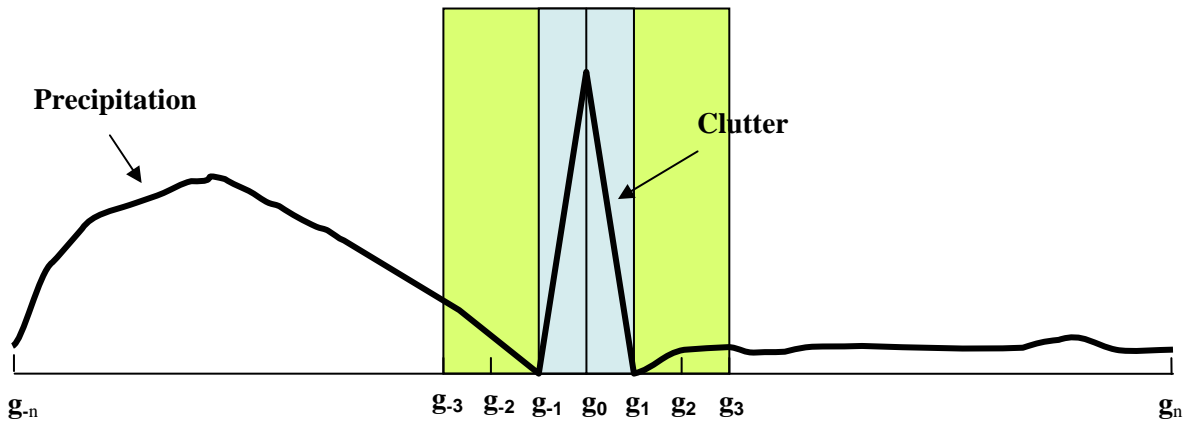

Figure 1. An idealized power spectrum that contains precipitation and clutter return. The velocity index is indicated by "g_i" with indices ranging from –n to +n, the limits of the Nyquist velocity. The blue region encloses the "clutter power" which corresponds to the power in the velocity indices of g_{-1}, g_0 and g_1, and is termed "C_p". The green regions contain the "power near zero" at the velocity indices of g_{-3}, g_{-2}, g_2 and g_3 and are termed "P_{nz}".
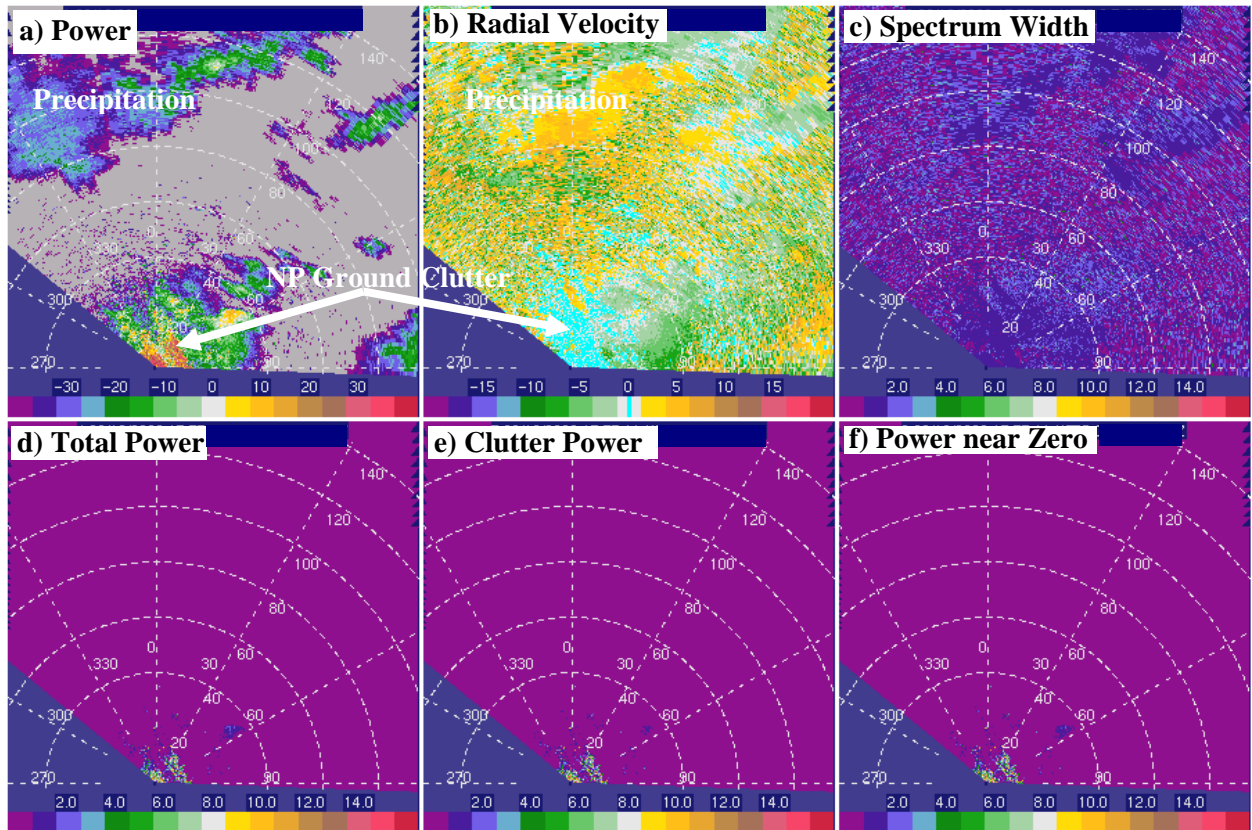
Figure 2. An example of spectral domain variables as calculated from KOUN time series data. Fields shown are a) reflectivity (dBZ), b) radial velocity (m s^{-1}) with values near 0 m s^{-1} shaded cyan, c) spectrum width (m s^{-1}), d) the total power (P_{tot}) field, e) the clutter power (C_p) field and f) the power near zero (P_{nz}) field. Notice the good discrimination between NP clutter and precipitation return.
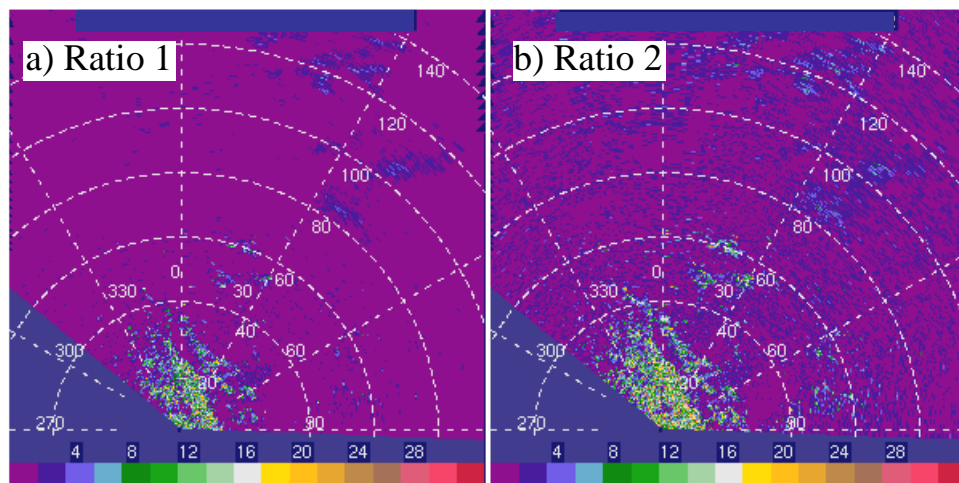

Figure 3. The results of the Ratio 1 and Ratio 2 calculations are shown for the KOUN data shown in Fig. 2.
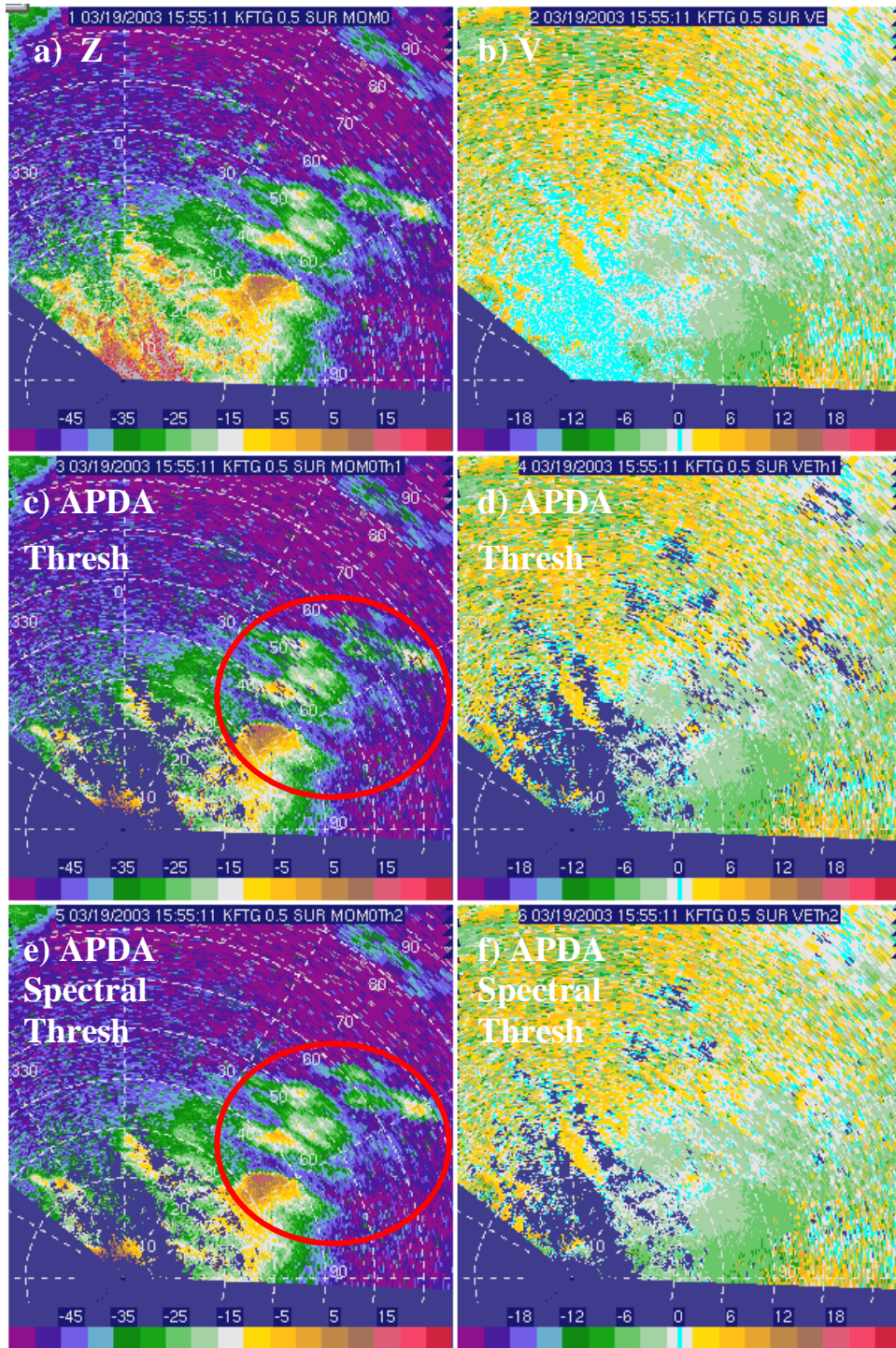
Figure 4. Comparison of the KOUN reflectivity and radial velocity fields when the APDA and the APDA-spectral are used to threshold the fields. Fields shown include a) unthresholded reflectivity (dBZ), b) unthresholded radial velocity (m/s), c) reflectivity thresholded with the original APDA, d) radial velocity thresholded with the original APDA, e) reflectivity thresholded with the APDA-spectral version and f) radial velocity thresholded with the APDA-spectral version. All thresholds were applied at an interest value of 0.5. Red ovals enclose precipitation return.
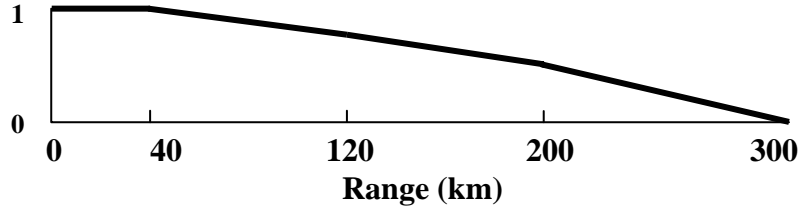
Figure 5. Range weight function used in RGDZ.

4.   Modified REC for the UAE Radars

For the UAE radars, a second version of the REC has been developed that includes a modified version of the AP clutter Detection Algorithm (mAPDA) and the Sea Clutter Detection Algorithm (SCDA). The SCDA defines regions of clutter caused by the radar beam interacting with the sea surface. The mAPDA and the SCDA were developed using data from the UAE C-band Doppler radars and were deployed for real-time operations in October 2002. In the future, the SCDA will be developed for the WSR-88D ORPG.

The mAPDA and the SCDA algorithms are described here and results presented.

4.1.   REC Feature Fields

An overview of the REC processes is given here. The base data fields of reflectivity (Z or DBZ), radial velocity (V), and spectrum width (W or SW) are input into the "feature generator" for calculation of derived fields called "features". Each of the REC algorithms uses a different combination of feature fields as input. A "membership function" is applied to the values of the feature fields to scale them to match the characteristics of the echo type under consideration. Membership functions are stepwise linear functions that scale the feature fields to have values between zero and unity. Output fields from this process are termed "interest fields". When an interest field has a value of 1.0, high likelihood exists that the echo type matches the desired characteristics; likewise, an interest value of 0.0 indicates no likelihood that the echo type matches the desired characteristics. Once the interest fields are calculated for all the algorithm feature fields, a weighted mean of all interest outputs is computed.

A threshold of 0.5 is desired for all REC algorithms.

All feature fields are calculated as a first step, and then each detection algorithm uses the pertinent features. With one exception, the features are computed over a small region typically defined as two beams on either side of the current beam and ± 1 km (Doppler fields) or ± 2 km (reflectivity fields) in range from the current gate. The vertical difference of the reflectivity (GDZ) is computed as a gate-to-gate difference. The following equations are used to calculate the REC features fields.

The "texture" of the reflectivity (TDBZ) field is the mean squared difference of the reflectivity and is calculated as shown in Eq. 6. For all equations that use reflectivity, the calculations are done in linear space.

$$TDBZ = \left(\sum_{j=1}^{Nbeams} \sum_{i=2}^{Ngates} \left(DBZ_{i,j} - DBZ_{i-1,j} \right)^2 \right) \Big/ (Ngates \times Nbeams)$$

Eq. 6

As described above, the vertical difference of the reflectivity (GDZ) field computes a gate-to-gate difference of the reflectivity values between two elevation angles as shown in Eq. 7.

$$GDZ = DBZ_{\substack{upper \\ angle}} - DBZ_{\substack{lower \\ angle}}$$

Eq. 7

For the SCDA, three feature fields have been devised that use the GDZ variable. First, it is used as specified in Eq. 7. Second, to allow for the presence of stratiform precipitation, the GDZ field is multiplied by the range weighting function (RangeWgt; Fig. 5) as specified in Eq. 8.

$$RGDZ_i = GDZ_i \times RangeWgt_i$$

Eq. 8

where i is the range gate number. Stratiform precipitation at long ranges from the radar will have large vertical differences in reflectivity values between elevation angles due to the shallow extent of the precipitation echo. The RGDZ feature field is an attempt to reduce these large differences at long ranges.

Third, GDZ is divided by the sine of the angular difference between the two elevation angles, as shown in Eq. 9, to calculate the vertical gradient of the reflectivity difference.

$$RSINZ_i = GDZ_i / [Range * \sin(\Theta_{upper\ angle} - \Theta_{lower\ angle})_i] \qquad \text{Eq. 9}$$

where i is the gate number along the beam and $Range$ is the radar range to the ith gate. For the same difference in reflectivity values between two elevation angles, the value of RSINZ will be larger at short ranges and smaller at long ranges.

The median radial velocity (MDVE) and the median spectrum width (MDSW) fields are calculated over the local area and used as feature fields. Using the median value has advantages over the mean value since the underlying structure within the field is preserved within noisy measurements.

The standard deviation of the radial velocity (SDVE) is calculated over the local area using Eq. 10.

$$SDVE = \left[\left(\sum_{j=1}^{Nbeams} \sum_{i=1}^{Ngates} \left(MDVE_{i,j} - \overline{MDVE} \right)^2 \right) \Big/ \left(Ngates \times Nbeams - 1 \right) \right]^{0.5}$$
$$\text{Eq. 10}$$

The *SPINchange* variable (also called SPIN) measures the number of changes in slope (i.e., first derivative sign changes) within the gate-to-gate reflectivity difference field, expressed as a percentage of all possible differences, that exceed the minimum difference (DBZ_{thresh}) allowed (Eq. 11). Steiner and Smith (2002) use a value of $DBZ_{thresh}=2.0$ for the WSR-88D data. For the REC (using S-Pol), the value of $DBZ_{thresh}=11.0$ to better distinguish clutter from precipitation.

For $\| (DBZ_i - DBZ_{i+1}) \| > DBZ_{thresh}$,

$SPINchange\_counts = SPINchange\_counts + 1$ and

$All\_counts = All\_counts + 1$.

For $\| (DBZ_i - DBZ_{i+1}) \| \le DBZ_{thresh}$, then

$All\_counts = All\_counts + 1$

$$SPINchange = \left\{ \frac{SPINchange\_counts}{All\_counts} \right\} x100 \qquad \text{Eq. 11}$$

However, *SPINchange_counts* is not incremented for $\| (DBZ_i - DBZ_{i+1}) \| > DBZ_{thresh}$ unless there has been a change in the slope of the reflectivity difference. For example, if the reflectivity difference is increasing along the beam and then decreases, *SPINchange_counts* is only incremented at the gate where the decrease begins.

4.2. mAPDA and SCDA Feature Fields

The feature fields used by the mAPDA include: TDBZ, MDVE, MDSW, SDVE, SPIN, GDZ, and RSINZ. The feature fields used for the mAPDA differ from those used for the WSR-88D APDA (see Kessinger et al. 2003). The GDZ and the RSINZ are added feature fields. Equal weights are used for all feature fields. Membership functions are shown in Fig. 6 with two of them differing slightly from those developed for the WSR-88D due to differing data characteristics of the EEC radars.

Feature fields selected for use by the SCDA include: TDBZ, MDSW, SDVE, SPIN, GDZ, RGDZ, and RSINZ. Because the vertical variation in reflectivity is such a strong indicator for sea clutter, three feature fields were devised with this indicator. Equal weights are used for each feature field. Membership functions are shown in Fig. 7. The SCDA is applied only over oceanic regions through the use of a terrain mask.
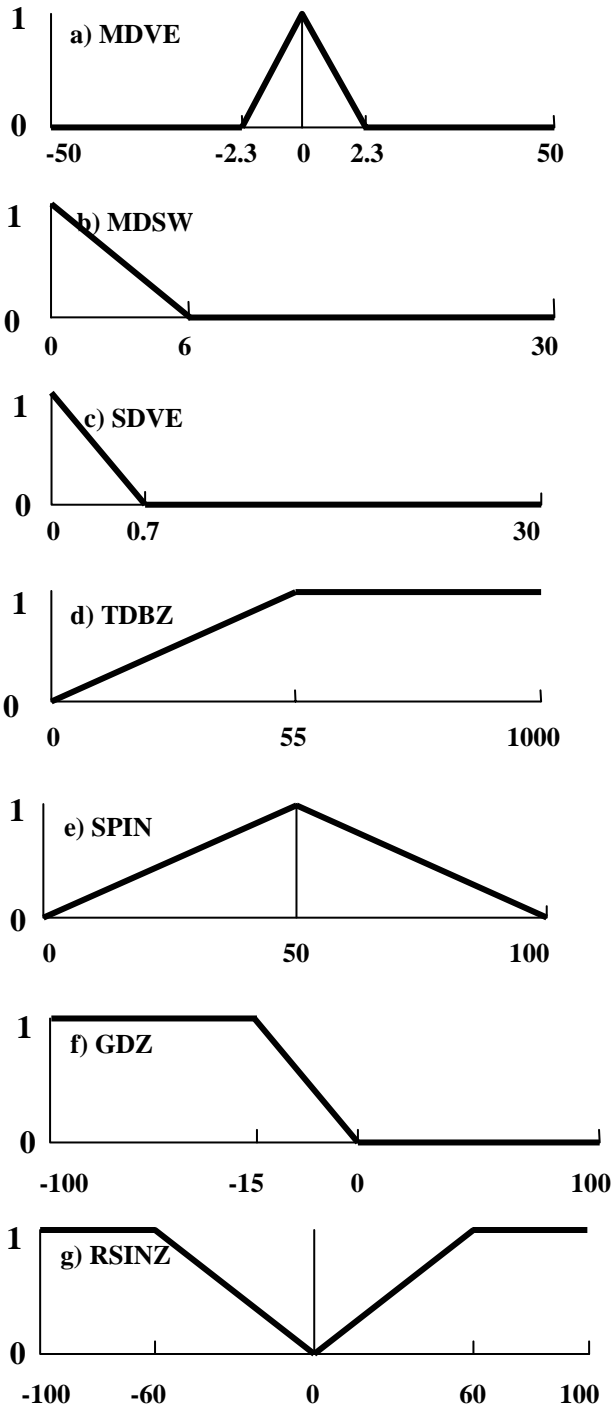
Figure 6. Membership functions for the modified AP clutter detection algorithm (mAPDA) as used on the UAE EEC C-band radars.
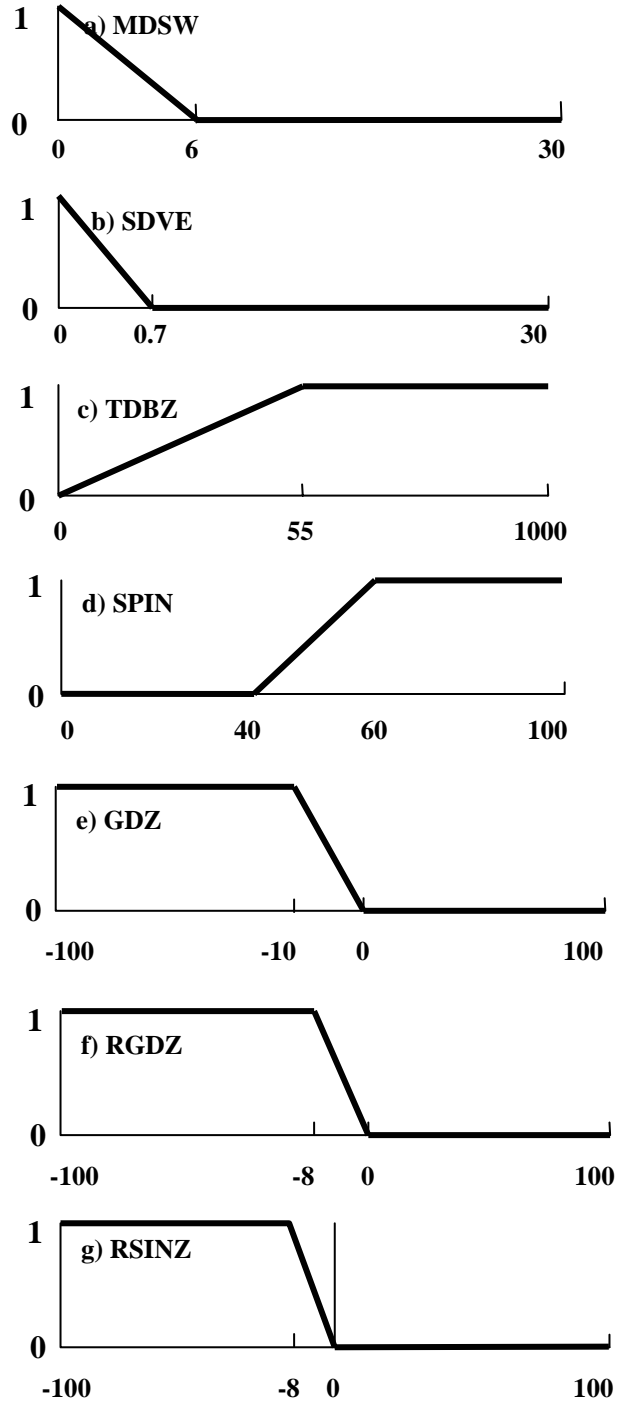
Figure 7. Membership functions for the sea clutter detection algorithm (SCDA) as used on the UAE EEC C-band radars.

4.3.   UAE Results

The locations of the five radars in the UAE are
shown in Fig. 8. The Arabian Sea and coastline
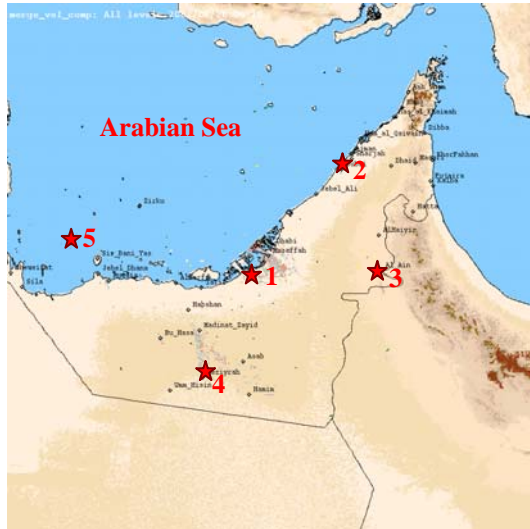features are common to all radar sites.

*Figure 8. This map shows the locations of the five
EEC C-band Doppler radars in the United Arab
Emirates. They are: 1) Al Dhafra, 2) Dubai, 3) Al
Ain, 4) Muzaira and 5) Dalma.*

Results from the modified REC (with mAPDA and
SCDA) are shown for three of the radars on
differing days. Each of the figures are organized in
the same manner with the original, unedited
reflectivity and radial velocity fields shown at the
top of the figure and the corresponding thresholded
reflectivity and radial velocity fields shown at the
bottom. The thresholding is accomplished with the
output from the mAPDA and the SCDA using a
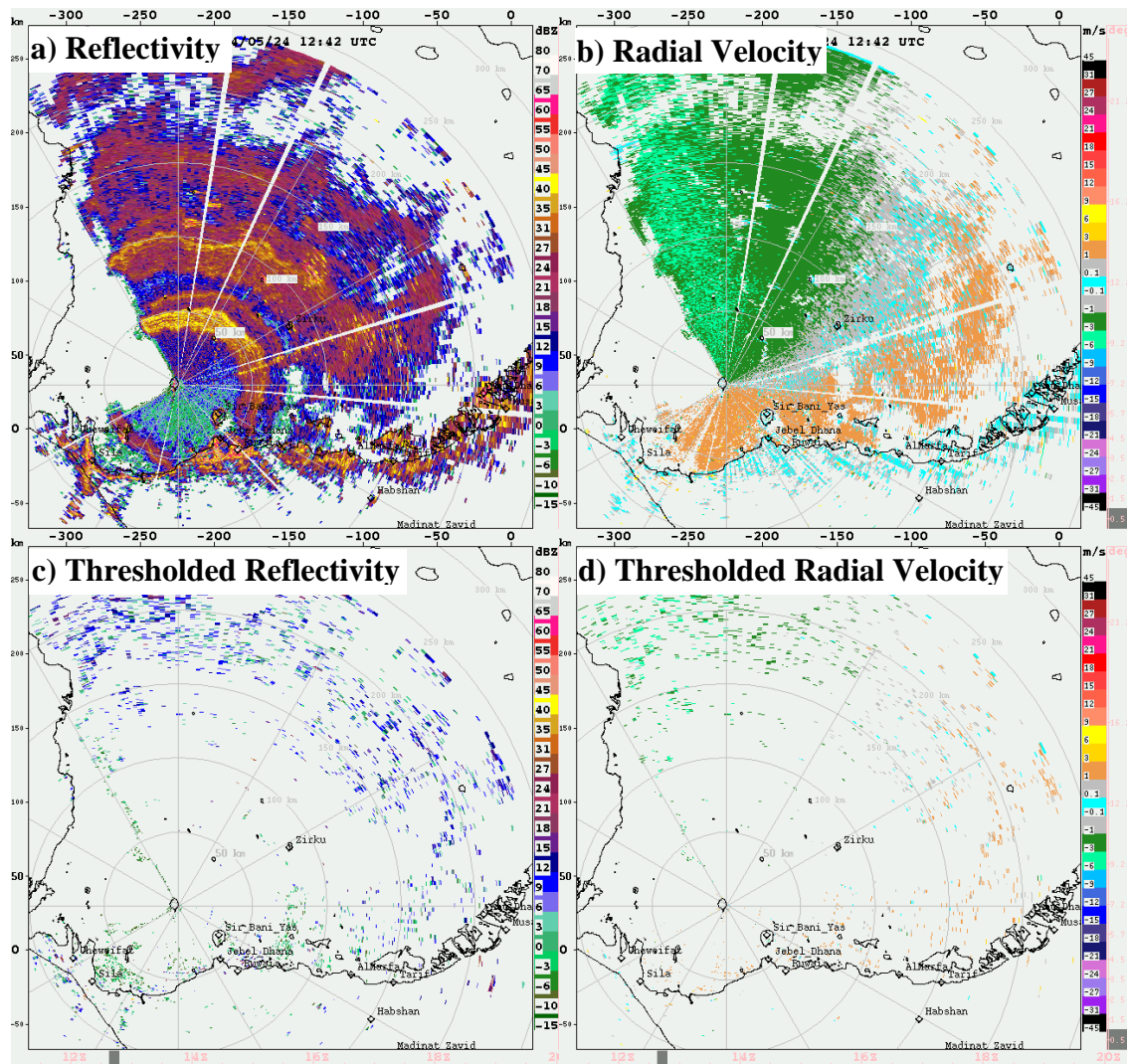threshold value of 0.5 for both.

Figure 9. Radar data from the Dalma radar are shown from 24 May 2004 at 1242 UTC at 0.5 deg elevation. Fields shown are: a) unedited reflectivity (dBZ), b) unedited radial velocity (m/s), c) reflectivity data thresholded with the mAPDA and the SCDA (dBZ) and d) similarly thresholded radial velocity data (m/s). Radial velocity values near zero m/s are shaded cyan. Range rings are at 50 km intervals.

The first example (Fig. 9) is taken from the Dalma radar on 24 May 2004 at 1242 UTC along the 0.5 deg elevation scan. The Dalma radar is sited on an island in the Arabian Sea, as shown in Fig.8. As seen in Fig. 9a and 9b, extensive sea clutter return is measured along with ground clutter from coastal features. The high reflectivity values in the sea clutter are especially striking as are the large regions of contamination. The mAPDA and the SCDA remove the majority of the contamination with scattered points remaining as seen in Fig. 9c and 9d. The remaining scattered points generally have a low reflectivity value of 15 dBZ and below.

Applying a de-speckling algorithm to the thresholded fields could further improve the results.
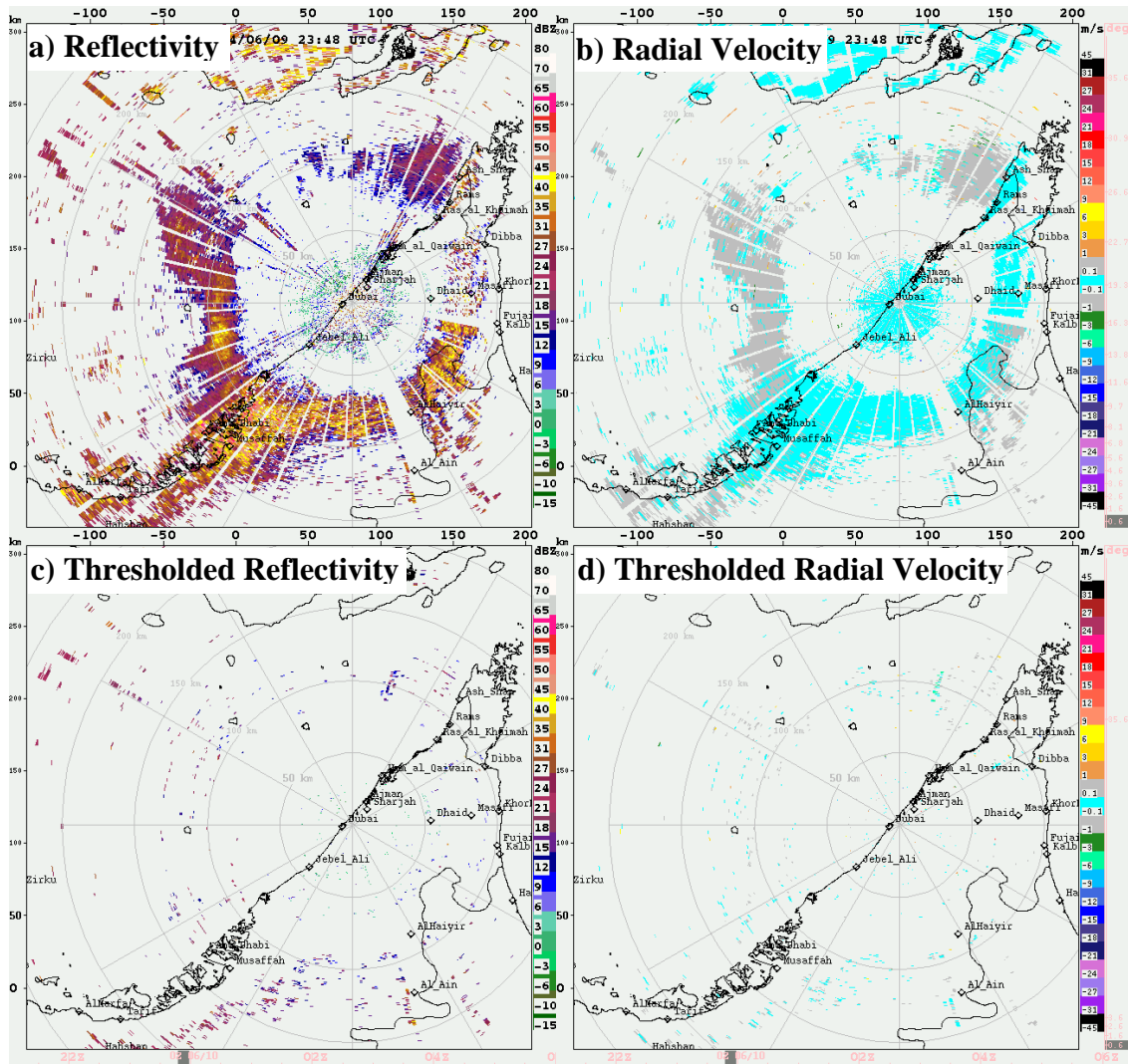
Figure10. Similar to Figure 9, radar data from the Dubai radar are shown from 9 June 2004 at 2348 UTC at 0.6 deg elevation.

A second example (Fig. 10) is shown using data from the Dubai radar on 9 June 2004 at 2348 UTC and along the 0.6 deg elevation scan. This case is also characterized by sea clutter and ground clutter returns as seen in Fig. 10a and 10b. The UAE REC removes much of the contamination (Fig. 10c and 10d) and leaves scattered points that could be mostly removed by a despeckling algorithm.
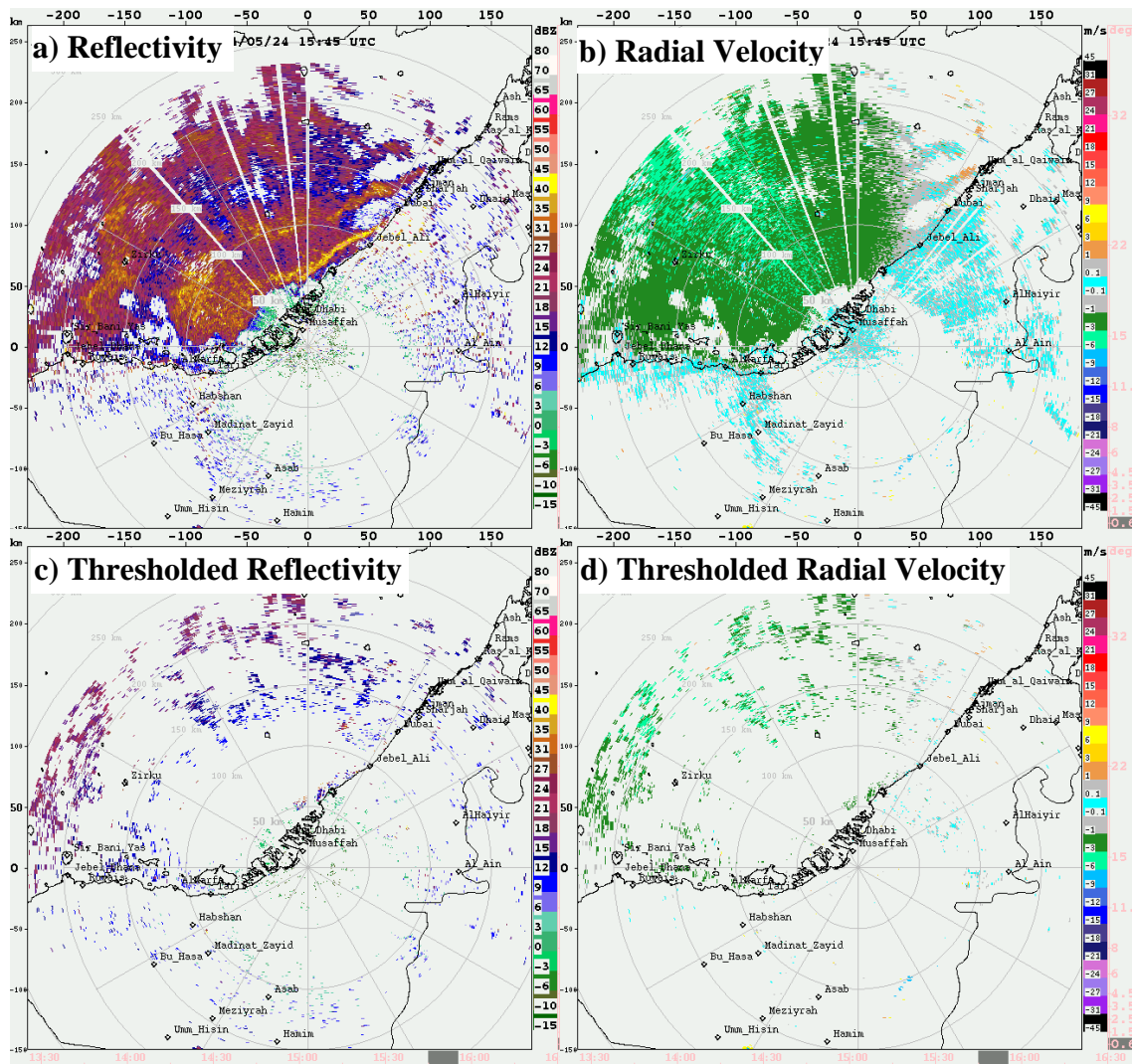
Figure 11. Similar to Figure 9, radar data from the Al Dhafra radar are shown from 24 May 2004 at 1545 UTC at 0.6 deg elevation.

The third and last case is taken from the Al Dhafra radar on 24 May 2004 at 1545 UTC (Fig. 11). The 0.6 degree elevation angle is shown. Like the other cases, extensive sea clutter is observed to the limit of the radar range, about 230 km (Fig. 11a and 11b). Clutter filters are in use for ground clutter return (over the land regions only) with the result that the reflectivity return consists of clutter-filter residual that can be seen near the coastline and inland as scattered, small regions of return. After application and thresholding of the mAPDA and SCDA, much of the sea clutter contamination is removed as are additional regions of the clutter-filter residual reflectivity (Fig. 11c and 11d).

These results show the effectiveness of the UAE

REC at removing contamination caused by ground clutter and sea clutter return.

5. Summary

An update on the AP Clutter Mitigation Scheme for the WSR-88D has been given. New spectral domain variables were input into the APDA. Results show that data quality improvement should be realized in the moment fields with the addition of spectral variables into the APDA. Migration of the APDA into the ORDA is being planned now.

The UAE version of the REC was presented and the mAPDA and the SCDA described. Results were shown for three cases of sea clutter and ground clutter contamination from three different

radars. The UAE REC has demonstrated its effectiveness at removing sea clutter and ground clutter contamination. The SCDA will be implemented in the ORPG at a future date.

6. Acknowledgements

7. References

Ellis, S.M., 2001: Compensating reflectivity for clutter filter bias in the WSR-88D, *Preprints, 17th Int'l IIPS Conf.*, AMS, Albuquerque, NM, 14-18 Jan 2001, 142-145.

Ellis, S., C. Kessinger, T.D. O'Bannon, and J. Van Andel, 2003: Mitigating ground clutter contamination in the WSR-88D. *Preprints-CD, 19th Int'l IIPS Conf.,* AMS, Long Beach, 9-13 Feb 2003.

Elvander, R.C., S.M Holt, B. Bumgarner and R. Ice, 2001: Weather surveillance radar – 1988 Doppler (WSR-88D) open radar data acquisition (ORDA) enhancements. *Preprints, 30th International Conference on Radar Meteorology*, American Meteorological Society, Munich, Germany, 19-24 July 2001, p. 694-697.

Fulton, R.A., J.P. Breidenback, D.J. Seo, D.A. Miller, and T. O'Bannon, 1998: The WSR-88D rainfall algorithm. *Weather and Forecasting*, **13**, 377-395.

Keeler, R.J., J. Lutz and J. Vivekanandan, 2000: S-Pol: NCAR's polarimetric Doppler research radar, *IGARRS-2000, IEEE*, Honolulu, HI, 24-28 Jul 2000, 4pp.

Keeler, R., J. Hubbert, and J. Lutz, 2003: NEXRAD data quality by spectral processing, Spectral processing on NCAR's S-Pol radar. *Preprints, IGARSS-2003*, Toulouse, France, 21-25 July 2003.

Kessinger, C., S. Ellis, and J. Van Andel, 1999: A fuzzy logic, radar echo classification scheme for the WSR-88D. *Preprints, 29th International Radar Meteorology Conference*, American Meteorology Society, 12-16 July 1999, Montreal, Canada, 576-579.

Kessinger, C., S. Ellis, and J. Van Andel, 2002: NEXRAD Data Quality: An update on the AP clutter mitigation scheme. *Preprints, 18th International Conference on Interactive Information and Processing Systems (IIPS) for Meteorology, Oceanography, and Hydrology*, American Meteorological Society, Orlando, 13-17 January 2002, p. 127-129.

Kessinger, C., S. Ellis and J. Van Andel, 2003: The radar echo classifier: a fuzzy logic algorithm for the WSR-88D. *Preprints-CD, 3rd Conf. Artificial Applications to Environmental Science,* AMS, Long Beach, 9-13 Feb 2003.

Kosko, B., 1992: *Neural Networks and Fuzzy Systems: A Dynamical Systems Approach to Machine Intelligence.* Prentice-Hall, N.J.

O'Bannon, T., 1998: The enhanced WSR-88D precipitation processing subsystem. Preprints, 14th International Conference on Interactive Information and Processing Systems (IIPS) for Meteorology, Oceanography, and Hydrology, American Meteorological Society, Phoenix, AZ, 11-16 Jan. 1998, 267-270.

O'Bannon, T., and F. Ding, 2003: Continuing enhancement of the WSR-88D precipitation processing subsystem. *Preprints, 31st Int'l Conf. on Radar Meteorology,* AMS, 6-12 August 2003.

Saffle, R.E., M.J. Istok and L.D. Johnson, 2001: NEXRAD open systems – progress and plans. *Preprints, 30th International Conference on Radar Meteorology,* American Meteorological Society, Munich, Germany, 19-24 July 2001, p. 690-693.

Smith, P.L., 1984: Equivalent radar reflectivity factors for snow and ice particles, *Journal of Climate and Applied Meteorology,* **23,** 1258-1260.

Steiner, M., R.A. Houze, Jr., S.E. Yuter, 1995: Climatological characterization of three-dimensional storm structure from operational radar and rain gauge data. *Journal of Applied Meteorology,* **34,** 1978-2007.

Super, A.B., and E.W. Holroyd, 1997: Snow accumulation algorithm development for the WSR-88D radar. *Preprints, 28th Conf. Radar Meteorology,* AMS, Austin, 7-12 September 1997, 324-325.